NJC

Accepted Manuscript

This is an *Accepted Manuscript*, which has been through the Royal Society of Chemistry peer review process and has been accepted for publication.

Accepted Manuscripts are published online shortly after acceptance, before technical editing, formatting and proof reading. Using this free service, authors can make their results available to the community, in citable form, before we publish the edited article. We will replace this *Accepted Manuscript* with the edited and formatted *Advance Article* as soon as it is available.

You can find more information about *Accepted Manuscripts* in the Information for Authors.

Please note that technical editing may introduce minor changes to the text and/or graphics, which may alter content. The journal's standard Terms & Conditions and the Ethical guidelines still apply. In no event shall the Royal Society of Chemistry be held responsible for any errors or omissions in this *Accepted Manuscript* or any consequences arising from the use of any information it contains.

ROYAL SOCIETY OF CHEMISTRY

www.rsc.org/njc

NJC

RSCPublishing

ARTICLE

The comparison of two classes of bifunctional SBA-15 supported platinum-heteropolyacid catalysts for the isomerization of *n*-hexane

Cite this: DOI: 10.1039/xoxxoooooox

Received ooth February 2015,
Accepted ooth February 2015

DOI: 10.1039/xoxxoooooox

www.rsc.org/

Teresa Pinto,[a] Philippe Arquillière,[a] Gerald P. Niccolai,[b] Frédéric Lefebvre*,[a] and Véronique Dufaud*,[a]

Mono- and bifunctional catalysts composed of silicotungstic acid ($H_4SiW_{12}O_{40}$) and/or platinum nanoparticles supported on SBA-15 mesostructured silica were comparatively tested for the isomerization of *n*-hexane. Monofunctional catalysts were produced by impregnating the SBA-15 support with either $H_4SiW_{12}O_{40}$ or the platinum particle precursor, H_2PtCl_6. In the bifunctional catalysts, both metallic and acid functions were combined either by mechanically mixing the monofunctional solids yielding a *multiphase* bifunctional material (**HSiW/SBA-15 + Pt/SBA-15**), or by dual impregnation of $H_4SiW_{12}O_{40}$ and Pt within a single material leading to the *monophasic* bifunctional catalyst, **HSiW/Pt/SBA-15**. These hybrid materials, with the exception of the monofunctional platinum catalyst, were all active for the gas-phase isomerization of *n*-hexane. The two bifunctional catalyst systems showed high activity and selectivity for branched isomers with no catalyst degradation over 3 days of reaction.

Introduction

Skeletal isomerization of linear paraffins (C_5-C_6) is a key refining process producing clean gasoline. The reaction consists in the transformation of straight-chain paraffins into branched-chain isomers without cracking, thus improving the overall octane number (RON) of hydrocarbon fuels. High octane number allows for better fuel combustion which means better performance of internal combustion engine.[1,2] Thus, improved technology for alkane isomerization can provide for higher performance gasoline with reduced reliance on highly regulated additives such as aromatics, olefins or methyl tert-butyl ether (MTBE).[1,2]

An on-going challenge in this field of research seeks the development of highly active catalysts for *n*-alkanes isomerization capable of operating under moderate temperatures while keeping high selectivity towards branched isomeric products. Indeed, under these mild reaction conditions, the thermodynamic equilibrium favors high concentrations of branched isomers.[3] For instance, in the particular case of *n*-hexane, isomerization to mono-branched products such as 2-methylpentane (2MP) and 3-methylpentane (3MP) would raise the octane number from 25 to 74. Further ramification to the di-branched dimethylbutane isomers (2.2DMB and 2.3DMB) leads to octane numbers of around 100.

The isomerization of linear alkanes is generally carried out over bifunctional catalysts comprising a metallic phase with hydrogenating/dehydrogenating properties and an acid phase on which isomerization and/or cracking may occur. The metal phase, in the presence of hydrogen, allows for a better stabilization of the catalytic activity as well as significant enhancement of the selectivity for isomerization by disfavoring the bimolecular mechanism pathway responsible of coke formation.†,[4] Nowadays, the industrial catalysts consist of platinum supported on chlorinated alumina or acidic zeolites such as H-mordenite.[5,6] Although the former can operates at temperatures as low as 120-180°C, it is highly sensitive to contaminants in the feed (i.e. water, sulfur) and requires additional chlorine treatment to maintain stable acidity and hence constant activity. On the other hand, zeolites are relatively stable with respect to poisoning by water and sulfur,[5,6] but less acidic than chlorinated alumina. As a

consequence, zeolites require more stringent operating conditions (220-400 °C, 15-30 bar H_2) for the activation of C_5-C_6 alkanes, which in turn is unfavorable for the production of branched isomers.[7-10] More recently, other solid acid materials, displaying stronger acid strength than zeolites, have been successfully applied to the skeletal isomerization of light alkanes. These include sulfated zirconia,[11,12] tungstated zirconia[13] and heteropolyacids (HPA)[14-17] among others.

HPA are particularly well-suited as catalysts for the isomerization of *n*-alkanes owing to their very strong Brønsted acidity and high thermal stability. In the past few years, several catalytic studies were undertaken using HPA in combination with a noble metal, mainly platinum, to perform the skeletal isomerization of *n*-alkanes in the C_4-C_{10} range.[18-20] Generally, these bifunctional catalytic systems, whether supported or not, were able to provide high conversion and selectivity towards branched isomeric products.[21-25] In most of the cases, it was shown that promotion with platinum considerably improved the selectivity and the stability with time on stream. For instance, Miyaji et al. used Pt-$Cs_{2.5}H_{0.5}PW_{12}O_{40}$ catalyst for the isomerization of *n*-butane. The results showed high selectivity for isomerization products (> 90 %) suggesting that this catalyst operated through monomolecular mechanism pathway.[5] Ivanov et al. investigated the catalytic activity of systems based on Pt-HPW Keggin and Dawson tungstic acid supported on zirconia. High activity for *n*-hexane isomerization was achieved with yield and selectivity for *iso*-hexanes of respectively 80 % and 96-98 % at 190 °C.[22] However, in most of the cases, the initial structure of the HPW compounds was partially damaged due to the insufficient stability of initial acids in contact with the ZrO_2 support resulting in lower concentration of active sites. Lately, Gherib et al. described a promotion effect of reduced Pt-Ce oxides in the isomerization of *n*-hexane for silica supported Keggin-based HPA, which was attributed to enhanced hydrogenating/dehydrogenating properties of the final composites.[26] A similar promotion effect on *n*-pentane isomerization was observed by doping zirconia supported Pt-$H_3PW_{12}O_{40}$ catalysts with lanthanum or cerium. The benefit of La or Ce addition on activity and selectivity, although strongly dependent on the Pt loadings, was ascribed to a better dispersion of HPA over the solid surface.[27] In a series of publications, Xu et al. investigated in details the skeletal isomerization of *n*-pentane using Pt-HPA immobilized onto various oxides. With ZrO_2 as support, the conversion of *n*-pentane reached 65 % at 200°C and atmospheric pressure, which is nearly the equilibrium value, with 97 % selectivity.[4] When supported over high surface area SiO_2 or γ-Al_2O_3, a marked decrease in the catalytic performance was observed for the Pt-HPA bifunctional catalyst. The greater efficiency of the Pt-HPA/ZrO_2 catalyst was attributed to its ability to generate stronger acid sites and to promote the dispersion of noble metal.[27] The use of mesoporous silica materials such as MCM-41 and SBA-1 was also investigated by the same authors.[4] While SBA-1 based Pt-HPA catalyst exhibited the highest activity, no noticeable changes in selectivity was observed, the difference in activity probably arising from distinct textural properties (e.g. pore connectivity, surface area) of the supports.[4]

In a previous report, we have shown that SBA-15 type silica could also be a suitable carrier for use in isomerization reactions of light alkanes.[28] Compared to MCM-41 based materials, its large pore volume and diameter (up to 80 Å) and thick walls allow for better reactant and product diffusion as well as provide thermal and mechanical resistance which are key parameters in view of industrial applications. With respect to *n*-hexane isomerization, SBA-15 supported $H_3PW_{12}O_{40}$ (HPW) and $H_4SiW_{12}O_{40}$ (HSiW) were found to be efficient catalysts affording branched isomers with high selectivity (> 90 %), the supported silicotungstic acid being intrinsically more selective than its phosphotungstic acid counterpart. However, as already mentioned for monofunctional acid catalysts, in the absence of any noble metals, a deactivation of the catalysts was noticed with time on stream which was attributed to poisoning of acid sites by coke formation.

In this contribution, we explore the influence of noble metal addition on the activity and stability of our previous monofunctional acid materials and examine whether the proximity between HPA and platinum functions has an impact on the overall performance of the system for the isomerization of *n*-hexane. For this purpose, two approaches were developed to produce bifunctional Pt-HPA catalytic systems, either by the simple mixing of the two monofunctional solids (separate metallic and acidic phases), or by including both HPA and platinum functions within a single material made in a two-step process. Silicotungstic acid was used for its strong acidity and high selectivity for this reaction based on our previous results. Platinum was chosen for its well-known hydrogenating/dehydrogenating properties. The present work also investigates the effect that hydrogen, reaction temperature and gas flow rate have on activity and products distributions. Detailed physico-chemical characterization of the obtained materials before and after catalytic runs was carried out using different techniques. These include X-ray powder diffraction at small and wide angles, elemental analysis, High Resolution Transmission Electron Microscopy (HRTEM) and High Angle Annular Dark Field Scanning Transmission Electron Microscopy (HAADF-STEM), infrared spectroscopy, H_2 chemisorption and nitrogen adsorption.

Experimental

General

Tetraethoxysilane (TEOS), poly-(ethylene oxide)-poly(propylene oxide)-poly(ethylene oxide) block copolymer (Pluronic 123, MW: 5000), 12-silicotungstic acid hydrate ($H_4SiW_{12}O_{40}.xH_2O$), chloroplatinic acid hexahydrate ($H_2PtCl_6.6H_2O$) and *n*-hexane (≥ 99 % purity) were purchased from Aldrich Chemical and used without further purification. Anhydrous ethanol (≥ 99.9 % purity) was obtained from Carlo Erba. SBA-15 silica was prepared according to the procedure reported by Zhao et al.[29-31]

Preparation of monofunctional catalysts

The monofunctional acid catalyst, **HSiW/SBA-15**, was obtained, as previously described,[28] by simply impregnating the SBA-15 support with a methanol solution of $H_4SiW_{12}O_{40}.xH_2O$ (HSiW) to achieve the desired tungsten loading of ~ 25 wt. %. The preparation of the metallic catalyst, **Pt/SBA-15**, was carried out using $H_2PtCl_6.6H_2O$ as the metal precursor following the method recently described by Li et al.[32] Typically, a desired amount of $H_2PtCl_6.6H_2O$ was dissolved in 20 mL of ethanol and then dispersed drop by drop onto the SBA-15 support. The quantities were adjusted to reach a Pt loading of ~ 1 wt. %. The resulting suspension was stirred at room temperature overnight. After removal of the solvent, the solid was dried in an oven at 80 °C during 15 hours. The dried material was next pre-treated at 300 °C for 2 hours in a flowing N_2 atmosphere. As reported by the authors, this step is crucial in obtaining well-dispersed Pt nanoparticles into the SBA-15 channels. To further control the generation of Pt particles size in the 2-6 nm range, an additional reduction step (H_2 flow, 300 °C, 2 hours) was introduced at the end of the synthesis.

Preparation of bifunctional catalysts

Catalysts containing both acidic and metallic functional groups were prepared using two different approaches. The simplest method, the mechanical mixture, consists to finely grind in an agate mortar an appropriate amount of the two previous monofunctional powders to obtain the desired *multiphase* bifunctional catalyst, denoted (**HSiW/SBA-15** + **Pt/SBA-15**). In the second approach, both types of functions were combined in the same material following a two-step process, involving first the formation of the metallic phase prior to the introduction of the acid one. In a typical synthesis, the necessary quantity of HSiW to reach a W loading of ~ 25 wt. % was dissolved in 5 mL of distilled water and added drop wise over the monofunctional **Pt/SBA-15** material previously heat-treated at 300 °C. The slurry was stirred at 500 rpm at room temperature overnight. After elimination of the water, the solid was dried at 80 °C during 15 hours. Finally, the material was reduced at 300 °C under H_2 for 2 hours leading to the final monophasic bifunctional catalyst labeled as **HSiW/Pt/SBA-15**.

Catalysts Characterization

Low and wide-angle X-ray powder diffraction (XRD) data were acquired on a Bruker D5005 diffractometer using the Cu Kα monochromatic radiation ((λ = 1.54184 Å). N_2 adsorption-desorption measurements were performed on an ASAP 2020 Micromeritics system. The samples were evacuated at 350 °C for 12 hours prior to the experiment. The surface area was obtained from the BET equation and the pore size distribution was calculated by the BJH method applied to the desorption branch of the nitrogen adsorption/desorption isotherm. Fourier transform infrared (FT-IR) spectra were recorded from KBr pellets, in the 400-4000 cm^{-1} range, on a Nicolet 5700 spectrometer in the absorbance modes. Elemental analyses were made by ICP-AES with an ICP spectroflamme-D from a solution obtained by treatment of the solid catalyst with a mixture of HF, HNO_3 and H_2SO_4 in a Teflon reactor at 150 °C. The morphology of the supported catalysts and platinum nanoparticles was examined by HRTEM (High Resolution Transmission Electron Microscopy) and HAADF-STEM (High Angle Annular Dark Field Scanning Transmission Electron Microscopy) with a JEOL JEM 2100F microscope operating at 200 kV with a point to point resolution of respectively 0.23 nm and 0.19 nm. The size distribution histograms were obtained from the manual measurement with J Image of at least 200 different nanoparticles assuming a near spherical shape and random orientation. Log normal fits were used to approximate experimental size distribution histograms. The chemical composition of the samples was analyzed using the energy-disperse X-ray (EDX) method. Before observation, two methods were used to prepare the samples: the powders were i) suspended in toluene and transferred onto a Cu grid (200 mesh coated with Formvar and carbon films) or ii) embedded within an EPON resin. After polymerization, thin slices (90 nm) were cut by ultramicrotomy with a diamond knife. The slices were then deposited over Cu grids (200 mesh) previously coated with a holey-carbon film. The last method was performed on selected samples to better visualize the Pt nanoparticles present on the surface and for the HAADF-STEM images. The platinum dispersion was determined by chemisorption of hydrogen. The experiments were made on a Micromeritics ASAP 2020 instrument. The samples were first activated at 110 °C under vacuum for 1 h and then under hydrogen at 350 °C. Finally, nitrogen was passed on the samples at 350 °C in order to remove any adsorbed hydrogen. The isotherm was made at 55 °C after cooling the sample.

Catalytic tests

The *n*-hexane isomerization took place in a fixed bed dynamic flow reactor at atmospheric pressure. The introduction of gas (argon or hexane) was monitored by a Bronkhorst® mass flow-meter. The reaction products were analyzed online by gas chromatography (GC) equipped with a flame ionization detector (FID) and a nonpolar capillary column KCl/Al_2O_3 (Varian Capillary column; 50m x 530µm x 15µm). It was possible to sample the gas upstream and downstream of the reactor. The experiments were conducted during 12 hours or 72 hours at temperatures ranging between 140 and 200°C. Typically, the synthesized hybrid materials were carefully weighed and charged into a stainless steel ½" cylindrical reactor (inside diameter 1 cm and 20 cm of length) to produce a catalyst bed 5 cm thick. The reactor was then heated under a flow of argon (5 $mL.min^{-1}$) for 2 hours at 200 °C to remove any adsorbed water. If necessary, the reactor was re-equilibrated at the desired reaction temperature. The gas flow was then switched to hydrogen bubbled through hexane at room temperature which corresponds to a partial pressure of *n*-hexane of 151 mmHg (5 $mL.min^{-1}$, hexane/hydrogen ratio = 0.25). All light hydrocarbons excepting methane and ethane (which are minor products and neglected in the following calculations)

have been identified and standardized for the flow reactor under dynamic flow conditions. Mass concentration and GC peak area are directly correlated. Conversion is defined as the sum of the mass concentrations of all products (cracking and isomerization) divided by the sum of all the products and the remaining *n*-hexane reactant:

$$\boldsymbol{Conversion}\,(\%) = \frac{\sum[P_i]}{\sum[P_i] + [hexane]_{remaining}}$$

Selectivity of each product is the mass concentration of that product divided by the sum of all product mass concentrations:

$$\boldsymbol{Selectivity}_{P_i}(\%) = \frac{P_i}{\sum[P_i]}$$

These values were used to calculate the global selectivity to isomerization products and to cracking products reported in Tables 2-4 and the corresponding figures.

The relative molar fractions among C_6 products are of particular interest. This corresponds to the mass concentration of each C_6 isomer (*n*-hexane and the four C_6 isomerization products) divided by the sum of those concentrations.

$$\textbf{Molar Fraction}_{\textbf{C6 isomer}_i}(\%) = \frac{P_{C6\ isomer_i}}{\sum[P_{C6\ isomer_i}]}$$

Results and Discussion

Preparation and characterization of catalysts

The synthesis of highly dispersed Pt nanoparticles onto high surface area supports has recently attracted much interest.[33] In addition to metal dispersion, metal particles size is also known to greatly influence the activity, selectivity as well as the catalysts lifetime.[33] Several methods have lately appeared in the literature to prepare stabilized and nano-sized Pt nanoparticles in the range of 1-10 nm inside the cavities of SBA-15 mesoporous silica.[33] These include the conventional incipient wetness impregnation technique, the deposition-precipitation route, the *in-situ* incorporation of Pt colloids during the oxide synthesis, the ion-exchange method from an organically modified surface and the chemical vapor deposition of volatile metal compounds followed by their subsequent decomposition.[33] Among all these approaches, we have identified the method reported by Li et al. as a reliable and convenient way to provide Pt/SBA-15 catalysts with highly-dispersed Pt nanoparticles.[32] Using an adapted Li synthesis, we obtained our platinum hybrid material, **Pt/SBA-15**, with a platinum loading of 0.8 wt. %. Note that this loading is relatively low when compared to Li's materials.

The monofunctional acid catalyst, **HSiW/SBA-15**, was prepared as previously described[28] by impregnating the SBA-15 support with a methanol solution of $H_4SiW_{12}O_{40}{\cdot}xH_2O$ to produce a material with 25 wt. % tungsten. In the previous report,[28] this material was characterized by highly dispersed and intact Keggin units available for catalytic reaction.

The simplest bifunctional catalyst containing both acidic and metallic functional groups was obtained by finely grinding an appropriate amount of the tungsten monofunctional material with the platinum material in an agate mortar, resulting in the *multiphase* bifunctional catalyst, denoted (**HSiW/SBA-15 + Pt/SBA-15**).

In the second approach, metallic and acidic functions were combined according to a stepwise two-step process leading to the *monophase* bifunctional catalyst **HSiW/Pt/SBA-15** having approximately the same charge in tungsten and in platinum as the *multiphase* system mentioned above. The synthesis initially proceeds as for the monofunctional **Pt/SBA-15** material, with the addition of an aqueous solution of $H_4SiW_{12}O_{40}{\cdot}xH_2O$ before the final reduction step producing the *monophase* bifunctional catalyst, **HSiW/Pt/SBA-15**.

Mono- and bifunctional catalysts were characterized by various physico-chemical and spectroscopic techniques. The results showed highly ordered and well dispersed materials, as proved by X-ray powder diffraction (XRD) measurements. All catalysts exhibited typical diffractograms characteristic of hexagonally ordered mesophases with the presence of three well-resolved peaks in the 2θ-range of 0.6°-3° indexed as (100), (110) and (200) reflections (Supporting Information, Fig. S1). The presence of higher order reflections as well as the absence of significant changes in the *d*-spacing (Table 1) indicated that the long-range structuration of the materials was not affected upon functionalization and that the principle structural features of the SBA-15 silica matrix were retained. The wide-angle XRD patterns of catalysts are shown in Fig. S2 (Supporting Information). Neither mono- nor bifunctional catalysts displayed diffraction peaks in the 10-70° 2θ-range evidencing that both HSiW Keggin ions and Pt nanoparticles were finely dispersed throughout the solids. In the case of the *monophase* bifunctional catalyst, **HSiW/Pt/SBA-15**, it also demonstrates that the initial high Pt dispersion, achieved in the first step of the synthesis, was not notably affected by subsequent immobilization of the acidic HSiW phase.

The textural data derived from the BET analysis of nitrogen adsorption and desorption experiments are presented in Fig. S3 (Supporting Information) for pure SBA-15 and mono and bifunctional hybrids. All materials exhibited type IV isotherms characteristic of mesoporous materials with a steep capillary condensation loop appearing at a relative pressure range of 0.6 to 0.8 P/P_0 which suggests a narrow mesopore size distribution in the samples.[34,35] The absence of substantial shift in the inflection position when compared to parent SBA-15 indicated that the mean pore diameters remained relatively unchanged upon functionalization (75-77 Å for hybrid materials versus 75 Å for plain SBA-15, Table 1). However, unlike **Pt/SBA-15**, HSiW derived materials, whether they contained or not Pt nanoparticles, showed a marked decrease in both specific surface areas and pore volumes with respect to parent SBA-15 (respectively from 859 m^2/g to 423-503 m^2/g and from 1.1 cm^3/g to 0.5-0.6 cm^3/g, Table 1) which is consistent with the

Table 1. Textural and physical properties of catalysts.

Catalyst	Pt (wt.%)	W (wt.%)	d_{100}[a] (Å)	a_0[b] (Å)	Wall thickness[c] (Å)	V_p[d] (cm^3/g)	V_μ[e] (cm^3/g)	D_p[f] (Å)	S_{BET} (m^2/g)	C_{BET}[g]
SBA-15	-	-	99	114	48	1.1	0.06	75	859	151
Pt/SBA-15	0.8	-	101	116	52	1.1	0.06	76	844	168
HSiW/Pt/SBA-15	0.7	22	99	115	50	0.5	0.04	75	423	302
HSiW/SBA-15	-	25	97	112	47	0.6	0.04	77	503	266

[a] d(100) spacing (the error is estimated as 3 Å). [b] $a_0 = 2d(100)/\sqrt{3}$ Hexagonal lattice parameter calculated from XRD. [c] Calculated by a_0 – pore size. [d] Total pore volume at $P/P_0 = 0.980$. [e] Microporous volume determined using the t-plot method. [f] Pore size from adsorption branch applying the BJH pore analysis. [g] Derived from the BET equation of the nitrogen adsorption isotherms.

presence of a large extent of HSiW clusters in the pore channels. This was further demonstrated by the increase in the C_{BET} parameter (from 151 for SBA-15 to 302 and 266 for respectively **HSiW/Pt/SBA-15** and **HSiW/SBA-15**) indicating a change in the surface polarity due to the presence of HSiW species.

The FT-IR spectra of all materials are displayed in Fig. S4 (Supporting Information), together with those of bulk HSiW and bare SBA-15. The FT-IR spectra of the **HSiW/SBA-15** and **HSiW/Pt/SBA-15** catalysts clearly showed the characteristic bands of the Keggin ion at 978 (ν_{as}(W-Od)), 928 (ν_{as}(Si-Oa)), 878 (ν_{as}(W-Ob-W)), and 790 cm^{-1} (ν_{as}(W-Oc-W))[36] indicating that the structural integrity of the HSiW Keggin units was preserved in all cases during the preparation of the samples. A confirmation of this behavior was also obtained by measurement of the acidity of the **HSiW/SBA-15** system which was found to be highly acidic (Fig. S5 in Supporting Information).

Further insight on nanoparticles size and morphology, chemical composition and spatial distribution over the support was provided by transmission electron microscopy. Representative HAADF-STEM images of the platinum-derived catalysts (**Pt/SBA-15** and **HSiW/Pt/SBA-15**) after reduction are displayed in Fig. 1. In all cases, one can see that the highly ordered hexagonal structure of SBA-15 was retained after the preparation processes. The distribution of Pt particles in **Pt/SBA-15** was rather uniform with no obvious bulk aggregates of the Pt metal which is in good agreement with the wide-angle XRD data. The HRTEM micrographs revealed quasi-spherical shaped Pt particles, mainly located inside the channels of the SBA-15 host (Supporting Information, Fig. S6). The particles mean size estimated both from the Gaussian distribution of particles size and H_2 chemisorption measurement was found to be respectively 5 and 5.3 ± 1.0 nm which matches well the SBA-15 pore width of 7.6 nm derived from the BJH method. EDX chemical analysis performed over a large number of sample areas of **Pt/SBA-15** (Supporting Information, Table S1) showed that Pt particles were uniformly present over most of the ordered surface with, on average, 0.28 atom Pt per 100 atoms Si. This is consistent with the elemental analysis of a milligram scale sample of **Pt/SBA-15** which also showed a value of 0.25 atom Pt per 100 atoms Si for a Pt loading of 0.8 wt. %.

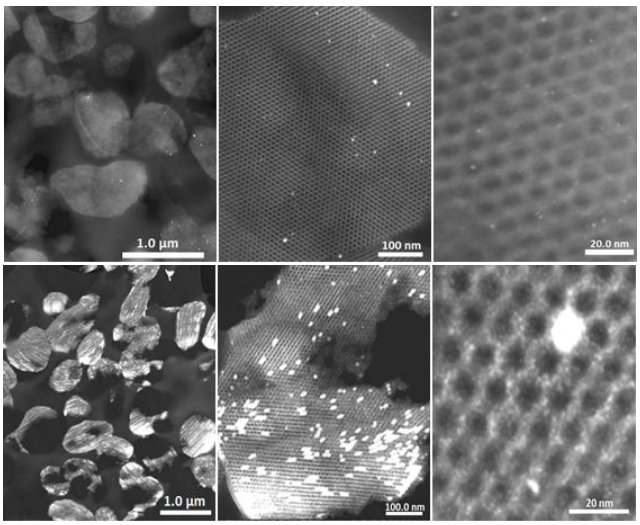

Fig. 1. Representative HAADF-STEM images of the platinum-derived catalysts: **Pt/SBA-15** (top) and **HSiW/Pt/SBA-15** (bottom).

The HAADF-STEM images of **HSiW/Pt/SBA-15**, taken at low magnification (Fig. 1, bottom, middle), showed an "island-type" distribution of the acidic HSiW phase over the whole surface with, in some cases, HSiW particles of 20-30 nm in diameter fulfilling some of the pores. At higher magnification, however, one can also observe some small bright areas at the surface or within the core of the silica framework, attributed to the presence of metallic clusters of 1-3 nm size (Fig. 1, bottom, right). EDX analysis confirmed the simultaneous presence of both Pt and W in these sample areas with a Pt/W atomic ratio varying between 0.04-0.08 which is a clear indication that both acidic and metallic functions in **HSiW/Pt/SBA-15** can coexist in very close proximity. HRTEM images of **HSiW/Pt/SBA-15** showed an average platinum nanoparticles size of 2.9 ± 1.1 nm (Supporting Information, Fig. S7) with a narrower particle size distribution when compared to **Pt/SBA-15** catalyst. This may be due to a better dispersion of the Pt nanoparticles during the

reduction step due to the presence of a large amount of HSiW (25 wt. % W). One can also evoke the synergistic participation of tungsten to the reduction process of Pt allowing for an easiest and fastest generation of Pt nanoparticles, and consequently much smaller Pt NPs.[37] Both **Pt/SBA-15** and **HSiW/Pt/SBA-15** catalysts revealed the presence of crystalline Pt particles. Comparison with known metallic and oxide Pt based structures and their synthetic protocols allows us probing the formation of metallic cubic Pt nanoparticles, as evidenced by the atomic resolution HRTEM micrograph and Fourier transform diffraction pattern exemplified for **Pt/SBA-15** in Fig. S8 (Supporting Information).

Catalytic results

In this study, our goal was to evaluate the performance of these different catalyst systems and probe more specifically the effect of bifunctional catalysts with respect to their monofunctional counterparts. Catalytic tests were performed by passing a carrier gas containing *n*-hexane through a bed of the solid catalyst in a dynamic reactor. Reactants and products were sampled at regular intervals. Some key basic performance results for each catalytic test are summarized in Table 2.

In a previous publication, we had shown that **HSiW/SBA-15** material was active for *n*-hexane isomerization but that the catalyst activity degraded with time on stream, which we attributed to the poisoning of acid sites by coke formation.[28] As aforementioned, several authors have proposed the introduction of hydrogen and hydrogenation catalysts to such systems to prevent coking. Thus, based on the optimal results from that study, **HSiW/SBA-15** was used as a catalyst for the isomerization of *n*-hexane in a hydrogen stream at 200 °C (Table 2, entry 1), with results similar to the previous reports. Initially, the catalyst showed moderate activity (12 % conversion) but this activity dropped steadily over the first 12 hours on-stream to 7 % (Fig. 2, top, square curve). This significant degradation is nevertheless less than that seen when using argon as a carrier gas. Selectivity increases slightly with time on-stream to achieve 93 % isomerization vs. 7 % hydrocracking after 12 hours on-stream (Fig. 2, bottom, square curve).

As expected, the monofunctional platinum catalyst **Pt/SBA-15** had no significant activity for *n*-hexane isomerization both initially and after 12 hours on-stream (Table 2, entry 2 and Fig. 2, top, triangle curve).

A marked improvement was immediately observed for a mechanical mixture of the two monofunctional materials, the *multiphase* bifunctional catalyst (**HSiW/SBA-15 + Pt/SBA-15**). This material showed high and steadily increasing *n*-hexane conversion (63 % after 12 hours on stream) with high selectivity for *n*-hexane isomers (96 %) with no measurable olefin formation (Table 2, entry 3). Under these reaction conditions, one can see that the distribution of *n*-hexane isomers approached the thermodynamic equilibrium mixture (*vide infra*, Table 3 and Fig. S10).

As previously stated, and demonstrated by other authors, the use of hydrogen is also a key to reduce coking. As a control, (**HSiW/SBA-15 + Pt/SBA-15**) was tested using argon as a carrier gas (Table 2, entry 4). In this case, *n*-hexane conversion after 12 hours was only 10 % with 93 % selectivity for isomerization. This performance is very similar to the monofunctional tungsten catalyst **HSiW/SBA-15** (Table 2, entry 1, 7 % conversion and 93 % selectivity), thus the presence of platinum does not have decisive effects on catalyst performance in the absence of hydrogen.

When using less of the monofunctional platinum catalyst in the mechanical mixture, thus reducing the overall platinum loading, conversion and selectivity were very slightly affected. The mixture of 0.5 g of **HSiW/SBA-15** with 0.05 g of **Pt/SBA-15** (0.04 wt. % Pt, Table 2, entry 5) produced 59 % conversion after 12 hours on stream (versus 63 % in entry 3) and 94 % selectivity (versus 96 % in entry 3). Thus, lesser quantities of platinum are sufficient to reduce catalyst degradation, and this point could be optimized if one were to pursue the use of the *multiphase* bifunctional catalysts.

Table 2. Conversions and selectivities of the mono- and bifunctional catalysts.

	Catalysts		Carrier	Conversion		Selectivity (12h)	
Entry	HPA Phase	Pt Phase	Gas	0 h	12 h	C_6	C_3-C_5
1	**0.5 g HSiW/SBA-15**	-	H_2	12	7	93	7
2	-	**0.5 g Pt/SBA-15**	H_2	0	0	-	-
3	**0.5 g HSiW/SBA-15**	**0.5 g Pt/SBA-15**	H_2	37	63	96	4
4	**0.5 g HSiW/SBA-15**	**0.5 g Pt/SBA-15**	Ar	15	10	93	7
5	**0.5 g HSiW/SBA-15**	**0.05 g Pt/SBA-15**	H_2	24	59	94	6
6	**0.5 g HSiW/Pt/SBA-15**		H_2	27	55	98	2

Reaction conditions: 1 bar, 200 °C, carrier gas flow 5 mL.min^{-1}, *n*-hexane partial pressure approximately 151 mmHg.

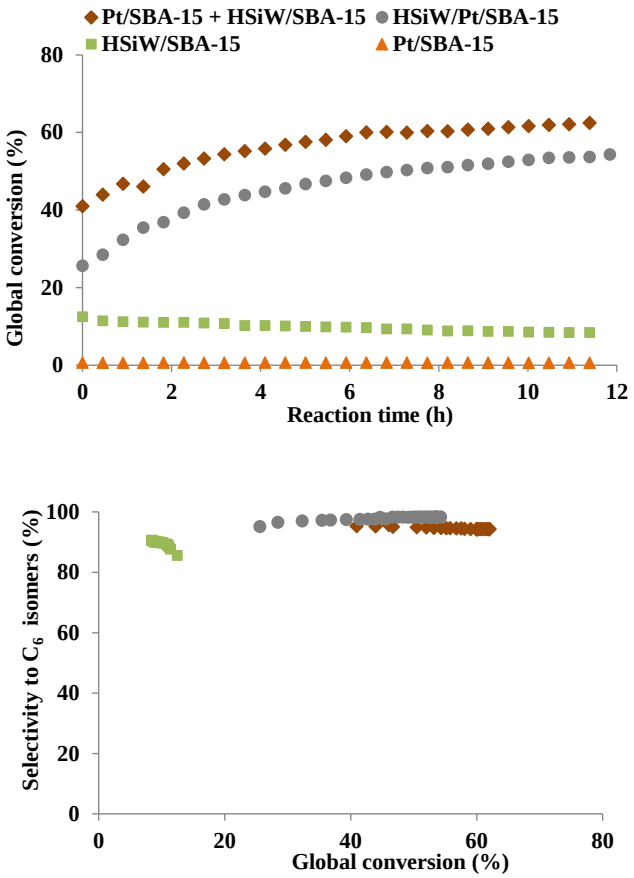

Fig. 2. Conversion of *n*-hexane as a function of reaction time (top) and selectivity to C_6 isomers as a function of the conversion (bottom) for mono- and bifunctional catalysts. Reaction conditions: 1 bar, 200 °C, 5 mL.min^{-1} hydrogen flow, hexane/hydrogen ratio = 0.25, catalyst (0.5 g). For the mechanical mixture, 0.5 g of each monofunctional catalyst was introduced.

The evolution of the stability of the *multiphase* bifunctional catalyst (**HSiW/SBA-15 + Pt/SBA-15**) was studied over a longer time on-stream, up to 80 hours (see Supporting Information, Fig. S9). Conversion continues to increase with time on stream, but the increases are very slight after 24 hours as one is approaching the thermodynamic equilibrium mixture of hexane isomers at this temperature (72 % conversion after 80 hours versus 86 % conversion at equilibrium). At this longer time-on-stream, one also observes that selectivity for isomerization is slightly decreasing as 0.2 % conversion to cyclohexane was detected.

To test the importance of platinum proximity to the tungsten site, the *monophase* bifunctional catalyst **HSiW/Pt/SBA-15** was also evaluated under similar conditions. Let's recall that this catalyst was prepared such that it contained approximately the same charge in tungsten and in platinum as the *multiphase* system (**HSiW/SBA-15 + Pt/SBA-15**) tested above. The *monophase* catalyst, **HSiW/Pt/SBA-15**, shows lower initial activity than (**HSiW/SBA-15 + Pt/SBA-15**) (27 % vs. 37 %, Table 2, entries 3 and 6), but again conversion steadily increases over time, closing the gap with that of the *multiphase* catalyst (Fig. 2, top, circle curve). Furthermore, selectivity of the *monophase* catalyst for *n*-hexane isomerization was superior to that of the *multiphase* catalyst at all conversions observed (Fig. 2, bottom, circle curve). Different explanations are available concerning these differences. For example, the proximity of platinum to tungsten could minimize diffusional limitations favoring rapid olefin hydrogenation once formed and, thus, reducing coking.

The presence of tungsten could also affect platinum dispersion during the catalyst reduction phase of the preparation of **HSiW/Pt/SBA-15**, leading to a more efficient hydrogenation catalyst. Indeed, HRTEM analysis (comparison Fig. S6 and S7) seems to indicate a smaller particle size for this material compared to the **Pt/SBA-15** catalyst used in the *multiphase* bifunctional system.

Comparative runs at varying temperatures were undertaken under isomerization conditions for the two bifunctional catalysts (**HSiW/SBA-15 + Pt/SBA-15**) and **HSiW/Pt/SBA-15** to determine the activation energy of the reaction and consider the distribution of isomers obtained in each case. The data were taken under steady-state conditions, that is, at 200 °C after 12 h reaction. Results are reported in Table 3.

For each catalyst, increasing the temperature leads to higher conversion of *n*-hexane but also to more lighter hydrocarbon cracking products. Similar results were obtained for Pt/HPW/ZrO_2 catalytic systems.[22] Overall, the *monophase* catalyst **HSiW/Pt/SBA-**

Table 3. Conversions and selectivities of multiphase and monophase bifunctional catalysts as a function of temperature.

Catalyst	T (°C)	Conversion (%)	Selectivity iC_6 (%)	Selectivity C_3-C_5 (%)	Mole fraction among C_6 compounds (%)				
					n-hexane	2,2-DMB	2,3-DMB	3-MP	2-MP
HSiW/SBA-15 + Pt/SBA15	140	7	98	2	93	0	1	4	2
	160	13	98	2	87	0	2	7	4
	180	37	98	2	63	1	4	20	11
	200	63	96	4	37	4	7	33	19
HSiW/Pt/SBA-15	160	9	99	1	90	0	1	6	3
	180	29	99	1	71	0	3	17	10
	200	55	98	2	45	2	6	30	18

Reaction conditions: 1 bar, 140-200 °C, carrier gas flow 5 mL.min^{-1}, hexane/hydrogen ratio = 0.25, 0.5 g catalyst (0.5 g of each monofunctional solids in the case of (**HSiW/SBA-15 + Pt/SBA-15**).

15 was slightly less active than the *multiphase* catalyst (**HSiW/SBA-15 + Pt/SBA-15**), but it was slightly more selective for isomerization of *n*-hexane over hydrocracking. The apparent activation energies calculated from these data (72 kJ.mol^{-1} for **HSiW/Pt/SBA-15** and 66 kJ.mol^{-1} for (**HSiW/SBA-15 + Pt/SBA-15**), Table S2 in Supporting Information) compare well with those reported for zeolites (around 60 kJ.mol^{-1}).[38]

Given the very high selectivity for isomerization over hydrocracking (between 1-4 % of reactor outflow depending on the experimental conditions) observed under these conditions, one can analyze the C_6 product distributions in a meaningful manner. Fig. S10 represents the data contained in Table 3 for C_6 products *only*, for each catalyst over several temperatures and the theoretical thermodynamic proportion of each product as a function of temperature.[39] This representation illustrates the reactivity difference between the catalysts noted above in the difference between the *n*-hexane curves, but one also notes that at 200 °C, some of the isomerization products are approaching their expected equilibrium values. Most notably, 2-methyl and 3-methyl pentane are at their expected values, while 2,3-dimethyl butane is not quite there, and especially the 2,2-dimethyl butane (or neohexane) is furthest from equilibrium. These phenomena are coherent with the conventional acid catalyzed monomolecular isomerization mechanism (Scheme 1). In the mechanism, methyl pentane products are produced by the first cycle of protonation and ß-methyl transfer. The dimethyl butane products (or the corresponding carbocations which lead to them) can only be formed from these initial products by a second ß-methyl transfer step. One also notes that 2,2-dimethyl butane, which Fig. S10 shows as being furthest from equilibrium, is formed via a secondary carbocation, whereas the other products are formed through presumably more stable tertiary carbocations.

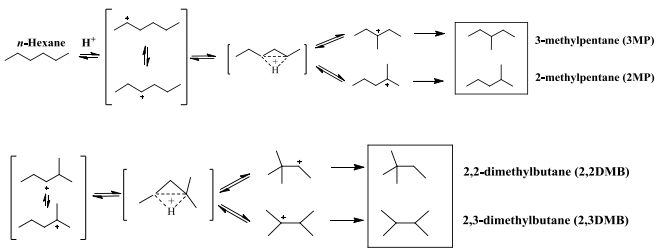

Scheme 1. Monomolecular mechanism of *n*-hexane isomerization over acid catalysts.

The dependence of catalyst performance and product distributions on contact time was probed by varying the flow rate of the substrate stream through the dynamic reactor for the *multiphase* bifunctional catalyst (**HSiW/SBA-15 + Pt/SBA-15**). Results are summarized in Table 4 and illustrated by Fig. S11. For comparison, Fig. S11 also plots the theoretical equilibrium values of molar fraction for each C_6 product at 200°C at zero flow rate (infinite contact time) on the horizontal axis.

As expected, in the predominance of *n*-hexane at the relatively low

Table 4. Conversions and selectivities of (**HSiW/SBA-15 + Pt/SBA-15**) as a function of contact time.

Catalyst	Flow rate (mL.min)	Conversion (%)	Selectivity iC_6 (%)	Selectivity C_3-C_5 (%)	Mole fraction among C_6 compounds (%)				
					n-hexane	2,2-DMB	2,3-DMB	3-MP	2-MP
HSiW/SBA-15 + Pt/SBA15	5	61	96	4	39	4	6	32	19
	10	50	97	3	51	2	6	26	16
	20	35	98	2	65	1	4	19	11

Reaction conditions: 1 bar, 200 °C, carrier gas flow 5-20 mL.min-1, hexane/hydrogen ratio = 0.25, 1 g of catalyst composed of 0.5 g of each monofunctional solids.

conversions produced under these conditions, conversion depends directly on flow rate, that is, the longer the effective contact time, the more *n*-hexane is converted. One also notes that at low flow rate, hydrocracking is slightly more significant. Concentrating on the isomerization product distributions (Fig. S11), one remarks that *n*-hexane, 2-methyl pentane, 3-methyl pentane, and 2,3-dimethyl butane selectivities all tend toward their expected thermodynamic equilibrium values whereas 2,2-dimethyl butane does not. This again is in accord with the monomolecular acidic isomerization mechanism in that the latter product is produced only through the formation of a secondary carbocation, which is unfavorable at this reaction temperature.

Characterization of catalysts after catalytic runs

Examination of the *mono-* and *multiphase* bifunctional catalysts after 3 days on stream showed high degree of hexagonal mesoscopic organization of the solids with no evidence of active phase clustering as demonstrated in the low- and wide-angle XRD patterns displayed in Fig. S12 and S13 (Supporting Information). The integrity of the HSiW Keggin ions was fully retained after reaction as assessed by FT-IR which exhibits the main bands associated with $H_4SiW_{12}O_{40}$ (Fig. S14). HRTEM measurements also indicated that the high initial dispersion of the Pt nanoparticles in these catalysts was maintained with no significant changes of the particle size distribution with average Pt particles size of 5.3 ± 1.7 nm and 2.3 ± 0.6 nm for respectively *multiphase* (**HSiW/SBA-15 + Pt/SBA-15**) and *monophase* **HSiW/Pt/SBA-15** catalysts (Fig. S15 and S16). Thus, these bifunctional catalysts proved to have excellent thermal behavior and stability under our reactions conditions.

Conclusions

Bifunctional Pt-HSiW catalysts supported onto SBA-15 silica were prepared using two different approaches, either by mechanically mixing monofunctional HSiW and Pt containing solids leading to separate metallic and acidic phases, or by including both HSiW and platinum functions nearby within a single material made in a two-step process. Hybrid materials with intact HSiW Keggin structures and highly dispersed Pt nanoparticles throughout the solid surface were produced as evidenced by FT-IR, XRD and HRTEM/STEM analyses. Both catalysts proved to be active for the gas-phase isomerization of *n*-hexane at 200 °C with conversion and selectivity for branched isomeric products superior to the monofunctional HSiW material, and furthermore that performance was maintained for long times on stream, in marked contrast to the monofunctional material. In the case of the mechanical mixture, even small amounts of platinum led to this increased performance, but only when the isomerization was carried out in the presence of hydrogen. Comparison between the two bifunctional catalyst systems showed that the *monophase* catalyst, **HSiW/Pt/SBA-15**, initially exhibited a lower activity than the multiphase bifunctional catalyst (**HSiW/SBA-15 + Pt/SBA-15**), but its activity steadily increased over time-on-stream toward that of the *multiphase* catalyst, but with clearly superior selectivity for isomerization. The study of various reaction parameters showed that 200 °C presents the best compromise between activity and the potential for hydrocracking reactions, and that given sufficient contact time, mixtures of C_6 products approaching thermodynamic equilibrium can be obtained. Characterization of used catalysts shows no evidence for catalyst modification after 3 days of reaction, further demonstrating their potential for industrial application.

Notes and references

[a] Laboratoire de Chimie, Catalyse, Polymères, Procédés
CNRS, Université Claude Bernard Lyon1, CPE Lyon
43 Bd du 11 novembre 1918, 69616 Villeurbanne cedex, France
Fax: (+33)472-431-795. E-mail: Veronique.Dufaud@univ-lyon1.fr; Frederic.Lefebvre@univ-lyon1.fr
[b] ICAR, UMR 5191 CNRS, Université Lumière Lyon 2, ENS Lyon, 15 parvis René-Descartes, 69342 Lyon cedex 07, France.

† In the bimolecular mechanism, the carbocation leads to an olefin which can further react with another carbocation yielding not only isomerization but also cracking through rearrangement and/or breaking of C-C bonds. Thus, the role of the Pt-H_2 system would be to reduce the alkene concentration by hydrogenation.

Electronic Supplementary Information (ESI) available: [XRD patterns before and after catalysis, nitrogen sorptions, FT-IR spectra, HRTEM images and evolution of C6 products as a function of temperature and flow rate]. See DOI: 10.1039/b000000x/

1 C. Marcilly, *Oil & Gas Sci.Technol.*, 2001, **56**, 499.
2 OPEC, *World Oil Outlook 2013*, Vienna, Austria, 2013.
3 R. A. Alberty, C. A. Gehrig, *J. Phys. Chem.*, 1984, **13**, 1173.
4 Y. Xu, X. Zhang, H. Li, Y. Qi, G. Lu, S. Li, *Catal. Lett.*, 2008, **125**, 340.
5 A. Miyaji, T. Echizen, L. Li, T. Suzuki, Y. Yoshinaga, T. Okuhara, *Catal. Today*, 2002, **74**, 291.
6 B. K. Modhera, M. Chakraborty, H. C. Bajaj, P. A. Parikh, *Catal. Lett.*, 2011, **141**, 1182.
7 M. Guisnet, L. Costa, F. R. Ribeiro, *J. Mol. Catal. A: Chem*, 2009, **305**, 69.
8 M. Guisnet, V. Fouche, M. Belloum, J. P. Bournonville, C. Travers, *Appl. Catal. A*, 1991, **71**, 295.
9 F. Ramoa Ribeiro, M. Guisnet, C. Marcilly, *Appl. Catal. A*, 1985, **13**, 281.
10 F. Ribeiro, C. Marcilly, M. Guisnet, *J. Catal.*, 1982, **78**, 267.
11 E. Iglesia, S. L. Soled, G. M. Kramer, *J. Catal.*, 1993, **144**, 238.
12 H. Liu, G. D. Lei, W. N. H. Sachtler, *Appl. Catal. A*, 1996, **137**, 167.
13 M. Hino, K. Arata, *J. Chem. Soc., Chem. Commun.*, 1988, 1259.
14 B. V. Sousa, K. D. Brito, J. J. N. Alves, M. G. F. Rodrigues, C. M. N. Yoshioka, D. Cardoso, *React. Kinet. Mech. Catal.*, 2011, **102**, 473.
15 E. Grinenval, A. Garron, F. Lefebvre, *Journal of Catalysts*, 2013, 828962, 8 pages.
16 Y. Liu, M. Misono, *Materials*, 2009, 2319.
17 J. Shanshool, U. Al-Rawi, *The 1st Regional Conference of Eng. Sci.*, 2008, **11**, 270.
18 N. Essayem, Y. Ben Taârit, C. Feche, P. Y. Gayraud, G. Sapaly, C. Naccache, *J. Catal.*, 2003, **219**, 97.
19 M. G. Falco, S. A. Canavese, R. A. Comelli, N. S. Fígoli, *Appl. Catal. A*, 2000, **201**, 37.
20 B. C. Gagea, Y. Lorgouilloux, Y. Altintas, P. A. Jacobs, J. A. Martens, *J. Catal.*, 2009, **265**, 99.

21 N. Essayem, Y. B. Taârit, P. Y. Gayraud, G. Sapaly, C. Naccache, *J. Catal.*, 2001, **204**, 157.
22 A. V. Ivanov, T. V. Vasina, V. D. Nissenbaum, L. M. Kustov, M. N. Timofeeva, J. I. Houzvicka, *Appl. Catal. A*, 2004, **259**, 65.
23 W. Kuang, A. Rives, M. Fournier, R. Hubaut, *Catal. Lett.*, 2002, **79**, 133.
24 W. Kuang, A. Rives, M. Fournier, R. Hubaut, *Appl. Catal. A*, 2003, **250**, 221.
25 X. Yang, J. A. Wang, L. Chen, S. P. R. Sebastian, A. M. Robledo, *Catal. Commun.*, 2012, **28**, 202.
26 A. Gherib, A. Aouissi, A. Rives, M. Fournier, R. Hubaut, *Chin. J. Catal.*, 2007, **28**, 1041.
27 Y. Xu, X. Zhang, H. Li, Y. Qi, G. Lu, S. Li, *Appl. Surf. Sci.*, 2009, **255**, 6504.
28 T. Pinto, V. Dufaud, F. Lefebvre, *Appl. Catal. A*, 2014, **483**, 103.
29 D. Zhao, J. Feng, Q. Huo, N. Melosh, G. H. Fredrickson, B. F. Chmelka, G. D. Stucky, *Science*, 1998, **279**, 548.
30 D. Zhao, Q. Huo, J. Feng, B. F. Chmelka, G. D. Stucky, *J. Am. Chem. Soc.*, 1998, **120**, 6024.
31 D. Zhao, J. Sun, Q. Li, G. D. Stucky, *Chem. Mater.*, 2000, **12**, 275.
32 N. Li, Z. Hu, M. Zheng, H. Lu, B. Zhao, S. Zhang, J. Zheng, G. Ji, J. Cao, *Mater. Lett.*, 2013, **106**, 193.
33 J. Zhu, T. Wang, X. Xu, P. Xiao, J. Li, *Applied Catalysis B: Environmental*, 2013, **130-131**, 197.
34 A. E. R. S. Khder, H. M. A. Hassan, M. S. El-Shall, *Appl. Catal. A*, 2012, **411-412**, 77.
35 K. Oh, S. Woo, *Catalysis Letters*, 2006, **110**, 247.
36 C. Rocchiccioli-Deltcheff, M. Fournier, R. Franck, R. Thouvenot, *Inorg. Chem.*, 1983, **22**, 207.
37 P. Arquillière, P. H. Haumesser, C. C. Santini, *Microelectron. Eng.*, 2012, **92**, 149.
38 M. M. Otten, M. J. Clayton, H. H. Lamb, *J. Catal.*, 1994, **149**, 211.
39 R. A. Alberty, *Chem. Eng. Sci.*, 1987, **42**, 2325.

SBA-15 supported bifunctional acidic HSiW-Pt catalysts proved to be active, stable and highly selective in the isomerization of *n*-hexane.